The iron-dopamine D1 coupling modulates neural signatures of working memory across adult lifespan

Jonatan Gustavsson[1], Jarkko Johansson[2], Farshad Falahati[1], Micael Andersson[4], Goran Papenberg[1], Bárbara Avelar-Pereira[1], Lars Bäckman[1], Grégoria Kalpouzos*[1], Alireza Salami*[1,3,4]

[1]Aging Research Center, Karolinska Institutet and Stockholm University, Sweden. [2]Umeå University, Faculty of Medicine, Department of Radiation Sciences, Sweden. [3]Wallenberg Center for Molecular Medicine at Umeå University [4] Department of Integrative Medical Biology, Umeå University, Umeå, Sweden

*Authors share the position as last authors.

Abstract

Brain iron overload and decreased integrity of the dopaminergic system have been independently reported as brain substrates of cognitive decline in aging. Dopamine (DA), and iron are co-localized in high concentrations in the striatum and prefrontal cortex (PFC), but follow opposing age-related trajectories across the lifespan. DA contributes to cellular iron homeostasis and the activation of D1-like DA receptors (D1DR) alleviates oxidative stress-induced inflammatory responses, suggesting a mutual interaction between these two fundamental components. Still, a direct in-vivo study testing the iron-D1DR relationship and their interactions on brain function and cognition across the lifespan is rare. Using PET and MRI data from the DyNAMiC study (n=180, age=20-79, %50 female), we showed that elevated iron content was related to lower D1DRs in DLPFC, but not in striatum, suggesting that dopamine-rich regions are less susceptible to elevated iron. Critically, older individuals with elevated iron and lower D1DR exhibited less frontoparietal activations during the most demanding task, which in turn was related to poorer working-memory performance. Together, our findings suggest that the combination of elevated iron load and reduced D1DR contribute to disturbed PFC-related circuits in older age, and thus may be targeted as two modifiable factors for future intervention.

Keywords: Dopamine, Iron, Working memory, Age, BOLD

Highlights

- First study demonstrating the association between regional iron and dopamine D1DR in adult humans.
- The interplay between age-related elevated iron and diminished D1DR explained lower task-related brain activity, which in turn was related to poorer task performance.
- Our findings iron-DA coupling can help progress the understanding of the mechanisms behind DA-related neurodegeneration.

1 Introduction

Aging is associated with cognitive decline (Gorbach et al., 2017; Salthouse, 2012) and concomitant alterations in structural, functional, and molecular properties of the brain (Andrews-Hanna et al., 2007; Bäckman et al., 2000; Gorbach et al., 2017; Zimmerman et al., 2006). Elevated iron content and decreased integrity of the dopaminergic system are typically reported as independent brain substrates of age-related cognitive decline (Bäckman et al., 2006, 2011; Cools & D'Esposito, 2011; Daugherty et al., 2015; Gustavsson et al., 2022; Hallgren & Sourander, 1958; Kalpouzos, 2018; Landau et al., 2009; Nyberg, Andersson, et al., 2009; Salami et al., 2019). Intracellular non-heme iron is involved in several fundamental neurobiological processes, including dopamine (DA) metabolism (Hare & Double, 2016; Mills et al., 2010). More specifically, iron is a cofactor of tyrosine hydroxylase during DA synthesis, indicating a critical role of iron in DA metabolism as well as in the development of the dopaminergic system (Erikson et al., 2001; Ortega et al., 2007; Unger et al., 2014; Zucca et al., 2017).

Iron is stored in the ferritin protein which keeps it from harming brain cells and is released upon metabolic demand. However, unbound iron accumulates with advancing aging and exerts detrimental effects on cellular integrity. Elevated iron content contributes to poorer myelin integrity (Steiger et al., 2016) and grey-matter atrophy (Daugherty & Raz, 2015, 2016), as well as altered frontostriatal activity (Kalpouzos et al., 2017; Rodrigue et al., 2020; Salami et al., 2021) along with disrupted functional connectivity in aging (Salami et al., 2018). Similar to consequences of elevated iron in aging, disruption of the DA system contributes to age-related neurocognitive impairment (Bäckman et al., 2006, 2011; Cools & D'Esposito, 2011; Landau et al., 2009; Nyberg, Dahlin, et al., 2009; Rieckmann et al., 2011; Salami et al., 2019). Given DA and iron are co-localized in high concentrations in the striatum, age-related iron dyshomeostasis combined with disturbance of the DA system may become harmful for brain integrity and cognition. Direct in-vivo studies testing the

59 synergistic effects between the dopaminergic system and iron on brain function and cognition in
60 aging are rare.

61 Past studies suggest that iron may cause neurotoxicity through DA oxidation, which may in turn
62 contribute to loss of dopaminergic neurons (Hald & Lotharius, 2005; Hare & Double, 2016; Youdim et
63 al., 1993; Zucca et al., 2017). Animal studies have demonstrated that iron-induced damage causing
64 DA depletion (Poetini et al., 2018) and deterioration of dopaminergic cells (Kaur et al., 2003) could be
65 restored after iron chelation. In contrast, a longitudinal study showed that dopaminergic cell death
66 precedes iron elevation in parkinsonian monkey (He et al., 2003). A study with young, middle-aged,
67 and older rhesus monkeys reported an association between iron and stimulus-evoked levels of DA
68 (Cass et al., 2007), with older monkeys exhibiting more iron accumulation and less DA release.
69 Although it remains unclear whether elevated iron is the cause or consequence of DA degeneration,
70 it is relatively well acknowledged in animal studies that these two key chemical components of the
71 brain interact with each other (Hare & Double, 2016).

72 As opposed to ample animal studies on iron-DA coupling, evidence for such an association across the
73 adult lifespan in humans is scarce. A recent longitudinal study showed that developmental changes in
74 pre-synaptic, but not post-synaptic, DA receptors were positively associated with iron accumulation
75 through adolescence and young adulthood (Larsen et al., 2020). Still, iron and DA play ambivalent
76 roles during early and later adulthood (Johansson et al., 2022; Kalpouzos et al., 2017; Salami et al.,
77 2021). Recent work showed that older individuals with genetic predisposition for lower DA (by proxy
78 of the *COMT* Val158Met genetic polymorphism) accumulated more iron in the dorsolateral
79 prefrontal cortex (DLPFC) and striatum over 3 years (Gustavsson et al., 2022). Postsynaptic DA
80 markers, particularly DA D1-like receptor (D1DRs) which are the most abundantly expressed receptor
81 subtypes, are among the most age-sensitive DA systems (Karrer et al., 2019). Moreover, the
82 activation of D1 and D2 receptors alleviates oxidative stress-induced inflammatory responses (Shao
83 et al., 2013; Yan et al., 2015; Zhu et al., 2018). Hence, with diminished DADRs, the capacity of the

protective response counteracting oxidative stress and neuroinflammation due to iron overload is lessened, and may lead to increased damage and ferroptosis (Hald & Lotharius, 2005).

Motivated by the lack of human studies, we investigated the relationship between dopaminergic receptors and iron content, and their interactions on brain function and cognition. Using the largest D1DR dataset across the world, we studied 180 healthy individuals (20-79 years old) who underwent D1DR Positron Emission Tomography (PET) assessment using [^{11}C]SCH23390, iron approximation made with magnetic resonance imaging (MRI) based quantitative susceptibility mapping (QSM; (Langkammer et al., 2012)), and functional magnetic resonance imaging (fMRI) while performing a working-memory task. We first examined regional variation in the link between D1DR and iron content with the hypothesis that greater iron content is related to lower D1DR, with a possible interaction with age (C.f. Salami et al., 2021; Kalpouzos et al.,2018). We targeted DLPFC and striatum, because of abundantly expressed D1DR (Shohamy & Adcock, 2010), pronounced age-related D1DR differences (Karrer et al., 2017), and association between *COMT* polymorphism (i.e., a dopaminergic gene) and iron accumulation reported in these regions (Gustavsson et al., 2022). Given the association of iron and DA to neural circuits of working memory (c.f., Salami et al., 2021; Salami et al., 2019), we predicted an interactive effect of iron and D1DR on load-dependent BOLD modulation and working memory processing (Gustavsson et al., 2022; Spence et al., 2020). To this end, we applied multivariate partial-least squares (PLS; ((McIntosh & Lobaugh, 2004)) which enables a simultaneous analysis of iron content, D1DR, age, on BOLD associations across all task conditions in a data-driven fashion. If these variables are simultaneously related to neural circuits of WM, PLS should reveal a single network showing that older individuals with elevated iron and decreased D1DR (i.e., toxic iron-DA coupling) exhibit lower task-related BOLD-response, particularly within the frontoparietal network. However, if D1DR and iron differentially modulate BOLD response (c.f., Salami et al., 2019; Salami et al., 2021), PLS should reveal different networks.

2 Materials and methods

This study uses data from the DopamiNe Age Connectome Cognition (DyNAMiC) project approved by the Umeå University Regional Ethical Board. All participants signed informed consent prior to data collection (for details about DyNAMiC, see Nordin et al., 2022).

2.1 Participants

One-hundred and eighty adults (mean age 49.8 ± 17.4 years; range 20-79; 90 females) from Umeå, Sweden, were recruited to participate in the project and underwent the full protocol, including cognitive testing, MRI, and PET assessments. All participants were native Swedish speakers, right-handed, and had no history of neurological illnesses. Of the sample of 180 participants, 3 dropped out of PET scanning, 4 were excluded due to incidental brain abnormalities, 3 due to failed reconstruction of QSM images. Additionally, brain and behavioural data were screened for univariate and multivariate outliers. Univariate outliers were defined as values greater or less than 3.29 SD from the mean (Tabachnick & Fidell, 2013) and excluded as pairwise deletions per ROIs and modality. Multivariate outliers were identified according to Mahalanobis distance ($p < 0.001$; Tabachnick & Fidell, 2013). As a result, five participants were identified as univariate outliers on their iron (n=3) or D1DR (n=2) values, and three were multivariate outliers. Thus, data from 162 individuals were used in the analyses involving iron content and D1D1R. Furthermore, three outliers were identified based on their online WM performance and excluded from analyses.

2.2 Neuroimaging acquisition and pre-processing

Participants underwent positron emission tomography on a Discovery 690 PET/CT scanner (General Electric) and MRI on a Discovery MR750 3.0 T scanner (General Electric) equipped with a 32-channel phased-array head coil at two separate occasions at Umeå University Hospital.

2.2.1 PET acquisition

PET was conducted to assess whole-brain D1DR using radioligand [^{11}C]SCH23390 at rest (for details see Nordin et al., 2022). The scanning session started with a low-dose CT image, followed by an

133 intravenous bolus injection of the radioligand. Participants were instructed to lay still and stay awake
134 with eyes open. An individually fitted thermoplastic mask was attached to the bed surface during
135 scanning to minimize head movement.

136 **2.2.2 Structural MR acquisition**

137 High-resolution anatomical T1-weighted images were acquired using 3D fast-spoiled gradient echo
138 sequence with the following parameters: 176 sagittal slices, slice thickness = 1 mm, voxel size 0.49 x
139 0.49 x 1 mm^3, repetition time (TR) = 8.2 ms, echo time (TE) = 3.2 ms, flip angle = 12°, field of view
140 (FOV) = 250 x 250 mm, no spacing.

141 **2.2.3 Iron acquisition**

142 Images for iron estimation was obtained using a 3D multi-echo gradient-recalled echo sequence
143 (meGRE). The parameters were as follows: 124 axial slices, voxel size 1 x 1 x 1.2 mm^3, TR = 31 ms, flip
144 angle = 17°, FOV = 256 x 256 mm, no spacing. The first TE was 1.78 ms followed by seven additional
145 TEs with a 2.87 ms interval.

146 **2.2.4 Functional MR acquisition**

147 The functional images were sampled using single-shot multiband EPI sequence with 37 axial slices,
148 voxel size 1.95 x 1.95 x 3.9 mm^3, 0.5 mm spacing, TR = 2.000 ms, TE = 30 ms, flip angle = 80°, and FOV
149 = 250 × 250 mm. Ten dummy scans were collected at the start of the sequence.

150 **2.2.5 In-scanner working memory task**

151 A numerical N-back task was administered in the scanner (Salami et al., 2018). A sequence of single
152 numbers appeared on the screen for 1.5s, with an interstimulus interval of 0.5s. During every item
153 presentation, subjects indicated whether the digit on the screen was the same as the one shown 1, 2,
154 or 3 digits back by pressing one of the two adjacent buttons with the index (Yes response) or middle
155 finger (No response). Each working-memory load condition (1-, 2-, and 3-back) was presented over
156 nine blocks in random order (interblock interval, 22 s) with each block consisting of 10 trials. For

every block, 10 trials were performed with four matches (requiring a "yes" response) and six nonmatches (requiring a "no" response). The N-back blocks were counterbalanced and trial sequence was the same for all participants. The maximum score for each condition was 81, 72, 63, respectively. Performance was calculated as an error-adjusted discrimination score by subtracting the proportion of false alarms (i.e., a wrong answer judged to be correct, or, in other terms, answering Yes, when the correct answer is No) from the proportion of correct hits (i.e., answering Yes when the correct answer is Yes).

2.2.6 PET processing

PET data obtained with [^{11}C]SCH23390 was processed with the following steps: To estimate receptor availability (i.e., D1DR) in targeted regions, binding potential relative to non-displaceable binding in a reference region (BP_{ND}; Innis et al., 2007) was used with cerebellum as reference. The processing of the PET data included correction for head movement by using frame-to-frame image co-registration, and co-registered with T1-weighted MRI data with re-slicing to MRI voxel size using Statistical Parametric Mapping (SPM12: Wellcome Trust Centre for Neuroimaging, http://www.fil.ion.ucl.ac.uk/spm/). To model the regional time-activity course (TAC) data we used simplified reference tissue model (SRTM; Lammertsma & Hume, 1996).

2.2.7 MRI processing

Quantitative susceptibility mapping. Processing of QSM is referred from Gustavsson et al. (2022). Approximation of iron content was inferred from susceptibility values derived from QSM images. Morphology-enabled dipole inversion (MEDI; T. Liu et al., 2011) is a method for QSM estimation that selects the solution that minimizes the discrepancy in the number of voxels belonging to edges between the susceptibility image and the magnitude image. Here, we used the recommended nonlinear variant of MEDI proposed by Liu et al. (2013). Initially, the total field map was estimated from the complex meGRE images by performing a nonlinear least square fitting on a voxel-by-voxel basis. The resulting frequency map was then spatially unwrapped using a guided region-growing

182 unwrapping algorithm (Xu & Cumming, 1999). The background fields, the superimposed field
183 contributions that are not caused by the sources inside the brain and mainly generated by air-tissue
184 interference, were eliminated using a nonparametric technique based on Projection onto Dipole
185 Fields (PDF: Liu et al., 2011). Finally, the corrected frequency map was used as input for the field-to-
186 source inverse problem to calculate susceptibility maps. The MEDI Toolbox
187 (http://weill.cornell.edu/mri/pages/qsm.html) was used to calculate QSM images.

188 Due to the singularity of dipole kernel at the centre of k-space, the generated QSM images contain
189 relative susceptibility values, which may not necessarily be comparable across subjects. To address
190 this issue, a region of the corticospinal tract was selected as a zero-reference region due to its
191 resilience to age-related degeneration (de Groot et al., 2015) and stable susceptibility across
192 adulthood (Li et al., 2014). Using white-matter areas as reference regions has previously been
193 recommended due to their low standard deviations of susceptibility, indicating low inter-subject
194 variation similar (Straub et al., 2017) or even lower than CSF (Deistung et al., 2013). The process of
195 zero-referencing is described in detail by Garzón and colleagues (2017).

196 Automated segmentation of cortical and deep gray-matter structures was performed with the
197 Freesurfer image analysis suite — version 6 (http://surfer.nmr.mgh.harva rd.edu/) using T1-weighted
198 images (Fischl et al., 2002; Fischl, Salat, et al., 2004; Fischl, Van Der Kouwe, et al., 2004).

199 Next, QSM and the segmentation results were resampled to the native structural space. Then,
200 statistics including average and standard deviation were computed on the QSM maps. We merged
201 segmented rostral and caudal middle frontal regions from the left and right hemispheres to form
202 DLPFC (Fig. 1A), and the left and right caudate and putamen to form striatum (supplementary
203 materials Fig. 1A).

204 Prior to computing statistics on the QSM maps, the boundary of segmentations was eroded by one
205 voxel, and a fraction (15%) of the most extreme values was removed to avoid the influence of high
206 signal from neighbouring vessels and obtain more robust estimates (Garzón et al., 2017).

2.2.8 Functional MRI processing

Pre-processing of the fMRI data, performed in SPM12 software, included slice-timing correction and motion correction by unwarping and re-alignment to the first image of each volume. The fMRI volumes were then normalized to a sample-specific template generated using Diffeomorphic Anatomical Registration using Exponentiated Lie algebra (DARTEL: Ashburner, 2007), affine alignment to MNI standard space, and spatial smoothing with a 6-mm full width at half maximum (FWHM) Gaussian kernel (voxel size = $2 \times 2 \times 2$ mm^3).

The pre-processed fMRI data were analysed with spatiotemporal PLS (McIntosh et al., 2004; McIntosh & Lobaugh, 2004) to assess the BOLD association with iron, D1DR, and age across the three experimental WM conditions (1-, 2-, and 3-back). PLS determines time-varying distributed patterns of neural activity as a function of experimental variables (1-, 2-, and 3-back) and regional iron and D1DR. This technique allows for the identification of patterns/networks, which reflect association changes across all regions of the brain simultaneously, rather than assemblies of independent regions, thus ruling out the need for multiple-comparison correction. A detailed description of spatiotemporal PLS analysis for fMRI data has been given in previous reports (Garrett et al., 2010; Grady & Garrett, 2014; Salami et al., 2010, 2012, 2014).

The onset of each stimulus within each block of images (1-, 2-, and 3-back) was averaged across blocks for each condition. A cross-block correlation matrix was computed as the correlation between neural activity across experimental conditions (1-, 2-, and 3-back) and variables of interest (age, D1DR, iron) across different regions. Then, the correlation matrix was decomposed using singular value decomposition (SVD), to identify a set of orthogonal latent variables (LVs) representing linear combinations of the original variables:

$$SVD_{CORR} = USV$$

This decomposition produces a left singular vector of regional susceptibility weights (U), a right singular vector of BOLD weights (V), and a diagonal matrix of singular values (S). This analysis

232 produces orthogonal LVs that optimally represent relations between the variables of interest (age,
233 D1DR, iron) and BOLD. Note that PLS is not mathematically susceptible to collinearity similar to the
234 multiple regression approach (Leibovitch et al., 1999). Each LV contains a spatial pattern exhibiting
235 the brain regions whose activity shows the strongest simultaneous relations to the input variables. To
236 obtain a summary measure of each participant's expression of a particular LV pattern, subject-
237 specific "brain scores" are computed by multiplying each voxel's (i) weight (V) from each LV (j) by the
238 BOLD value in that voxel for person (m), and summing over all (n) brain voxels:

$$\sum_{i=l}^{n} \mathrm{v}_{ij} \mathrm{BOLD}_{im}$$

239

240 Taken together, a brain score represents the degree to which each subject contributes to the
241 multivariate spatial pattern captured by a latent variable.

242 The statistical significance of each LV was assessed using permutation testing. This procedure
243 involved reshuffling the rows of the data matrix and recalculating the LVs of the reshuffled matrix
244 using the same SVD approach. The number of times a permuted singular value exceeds the original
245 singular value yields the probability of significance of the original LV (McIntosh et al., 1996). In the
246 present study, 1000 permutations were performed. In addition, the stability of voxel saliencies
247 contributing to each LV was determined with bootstrap estimation of standard errors (SEs), using
248 1000 bootstrap samples (Efron & Tibshirani, 1986). The Bootstrap Ratio (BSR: the ratio between
249 voxel saliences and estimated SEs) was computed and voxels with BSR > 3.29 (similar to a Z-score of
250 3.29, corresponding to p = 0.001) were considered reliable. All reliable clusters comprised contiguous
251 voxels, with a distance between clusters of at least 10 mm. Moreover, the upper and lower
252 percentiles of the bootstrap distribution were used to generate 95% confidence intervals (CIs)
253 around the correlation scores to facilitate interpretation (McIntosh & Lobaugh, 2004). For instance, a
254 significant difference between correlation scores in different conditions is indicated by non-

overlapping CIs. Similarly, brain or correlation scores were considered unreliable when CIs overlapped with zero.

PLS uses all conditions of an experiment and variables of interest at once, thus offering an additional dimension by simultaneously considering both similarities and differences across the experimental variables. If the variables of interest (i.e., age, iron content, D1DR) are similarly related to brain regions, PLS reveals a pattern with reliable loadings (with/without quantitative differences) for all variables. If a single variable dominates the pattern, PLS should reveal a reliable loading for that variable only. Alternatively, if different variables (e.g., D1DR and iron) differentially modulate BOLD response (e.g., Load-dependent effects of dopamine on BOLD as shown in Salami et al., (2019) versus load-independent effect of iron on BOLD shown in Salami et al., 2021), PLS may reveal two distinctive networks.

2.3 Additional statistical analyses

To assess age-effects on cognitive performance, a multivariate analysis of covariance (MANCOVA) was conducted with WM load-conditions as dependent variables and age-groups (younger (age 20-39) vs. middle-aged (age 40-59) vs. older (age 60-79)) as between-subjects factors. Follow-up independent t-tests were conducted to assess significant differences between age groups. To assess the relationship between iron content and D1DR, we conducted partial correlation analyses for each region of interest with iron content and D1DR as dependent variables, controlling for age. As control analyses, we performed the same analyses but included sex, education, and regional grey-matter volume as covariates.

3. Results

3.1 Demographics

Demographic information along with data on body mass index (BMI), brain volumes, D1DR, and N-back performance are presented in Table 1.

Table 1. Participant characteristics

		Mean	SD
N (Women)	162 (79)		
Age		50	17
Age range		20-78	
MMSE		28.8	1.1
BMI		25.2	3.9
Education		15	3.4
Volume[a]			
DLPFC		20478	2696
Striatum		11473	1282
Iron[b]			
DLPFC		0.0430	0.0140
Striatum		0.0998	0.0286
D1DR			
DLPFC		0.3582	0.0690
Striatum		1.6130	0.2182
WM performance			
1-back accuracy[c]		75.18	6.65
1-back (H-FA)[d]		0.86	
2-back accuracy		60.99	8.77
2-back (H-FA)		0.72	
3-back accuracy		48.10	9.57
3-back (H-FA)		0.59	

Note. MMSE = Mini Mental State Examination,
DLPFC = Dorsolateral prefrontal cortex, SD = Standard deviation.
[a] *Volume (mL) adjusted for total intracranial volume*
[b] *Approximation of iron, based on susceptibility in parts per million*
[c] *Accuracy calculated as the sum of correct responses*
[d] Proportion of false alarms (FA) subtracted from proportion of hits (H)

The MANCOVA conducted on N-Back performance showed a significant main effect on load conditions ($F_{2,155}$ = 228.24, $p < 0.001$, Wilk's $\Lambda = 0.253$, partial $\eta^2 = 0.747$), and an age-group effect on load conditions ($F_{4,310}$ = 9.43, $p < 0.001$, Wilk's $\Lambda = 0.795$, partial $\eta^2 = 0.108$). Post-hoc analysis for the lowest WM load (1-back) showed that the older participants performed less accurately compared to both middle-aged (t_{89} = -3.974, $p < 0.001$) and younger participants (t_{71} = -5.707, $p < 0.001$). There was no significant difference between younger and middle-aged participants ($p = 0.07$). For 2-back, older participants performed significantly poorer compared to both middle-aged (t_{105} = -4.015, $p < 0.001$)

302 and younger participants (t_{85} = -8.905, $p < 0.001$). Middle-aged participants performed significantly
303 poorer compared to younger participants (t_{98} = -4.176, $p < 0.001$). Lastly, for highest WM load (3-
304 back), older participants performed significantly poorer compared to both middle-aged (t_{105} = -5.300
305 $p < 0.001$) and younger participants (t_{102} = -7.950, $p < 0.001$). Middle-aged participants performed
306 significantly poorer compared to younger participants (t_{105} = -2.921, p = 0.004).

307 **3.2 Iron content in DLPFC, but not in striatum, was negatively associated with D1DR**

308 Both striatal and DLPFC iron increased with advancing age (striatum: r = 0.551, $p < 0.001$; DLPFC: r =
309 0.244, p = 0.002). D1DRs in both regions decreased with advancing age (striatum: r = -0.62, $p < 0.001$;
310 DLPFC: r = -0.565, p = < 0.001).

311 The partial correlation analysis for iron content and D1DR in DLPFC showed a significant negative
312 association across the whole sample (r = -0.272, $p < 0.001$), suggesting that greater iron content was
313 linked to lower D1DR (Fig. 1B). Further group level analyses revealed that this correlation was
314 similarly expressed across different age groups (Younger: r = -0.10, p = 0.48; Middle-aged: r = -0.30, p
315 = 0.026; Older: r = -0.37, p = 0.006). However, striatal iron content was unrelated to D1DR across the
316 whole sample (r = -0.101, p = 0.20; supplementary materials, Fig. 1B). No significant association was
317 observed within each age groups (Ps > 0.05), except for a trend-level link in the older individuals (r = -
318 0.24, p = 0.08).

319

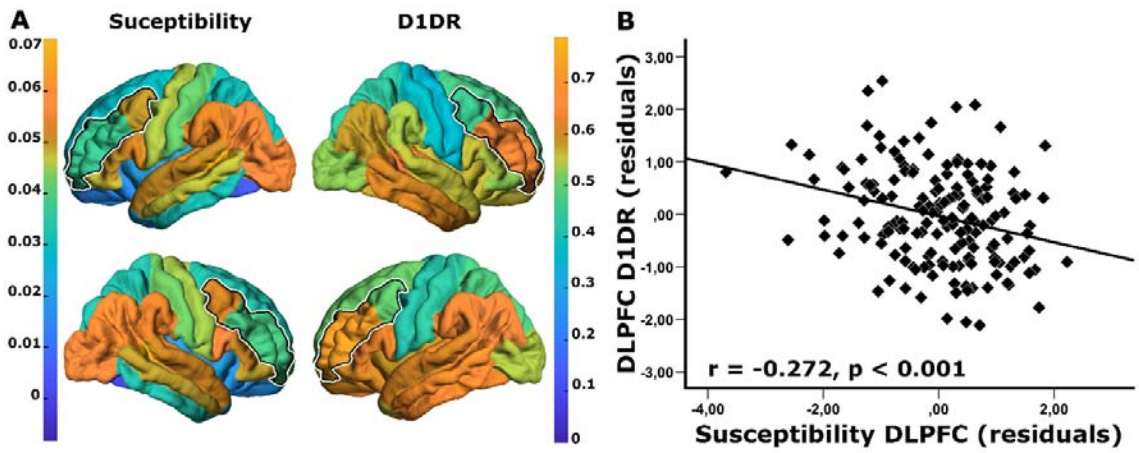

Figure 1. The relationship between iron content and D1DR in dorsolateral prefrontal cortex. **(A)** Surface map representing distribution of cortical iron (susceptibility in parts per million; left column) and D1DR ([^{11}C]SCH23390 BP_{ND}; right column) with dorsolateral prefrontal cortex (DLPFC) outlined. **(B)** Scatterplot depicting the association between greater iron content and lower D1DR in DLPFC. All values are z-transformed residuals adjusting for age.

3.3 Iron-D1DR couplings in DLPFC modulates WM-related BOLD in a load-dependent fashion

Given the iron-D1DR link in DLPFC, we next investigated whether iron-D1DR coupling modulated neural correlates of PFC-related function across the adult lifespan. We used behavioural PLS to assess the presence of multivariate spatial patterns of task-related BOLD response dependent on age, iron content, and D1DR across load conditions during N-back working memory task. The analysis identified two significant latent variables (LVs). LV1 represented a brain-wide network with increased activation in older individuals in a load-independent fashion. This network was largely unrelated to D1DR or iron in DLPFC (supplementary materials 5.1.2, Table 1, Fig 2).

The second LV represented the canonical WM network (c.f. Nagel et al., 2009; Salami et al., 2018). This LV (permuted p = 0.02, 17.97% of cross-block covariance: Fig. 3A) demonstrated that older individuals with elevated iron content and lower D1DR in DLPFC exhibited lower BOLD response in the frontoparietal network during 3-back (Fig. 3B). In contrast, higher BOLD response in the

339 frontoparietal network during 1-back was associated with older age and lower D1DR in DLPFC, but
340 not with iron content. For 2-back, no associations were considered reliable as the CI:s overlapped
341 with zero (Fig. 3B). As opposed to the frontoparietal WM network, the default-mode network (Fig. 3A
342 (Blue areas); supplementary Table 2) was less deactivated during 3-back in older individuals with
343 higher iron content and lower D1DR in DLPFC. Taken together, these results revealed that iron-D1DR
344 coupling modulates neural correlates of the working memory in a load-dependent fashion.

345

346

347

348

349

350

351

352

353

354

355

356

357

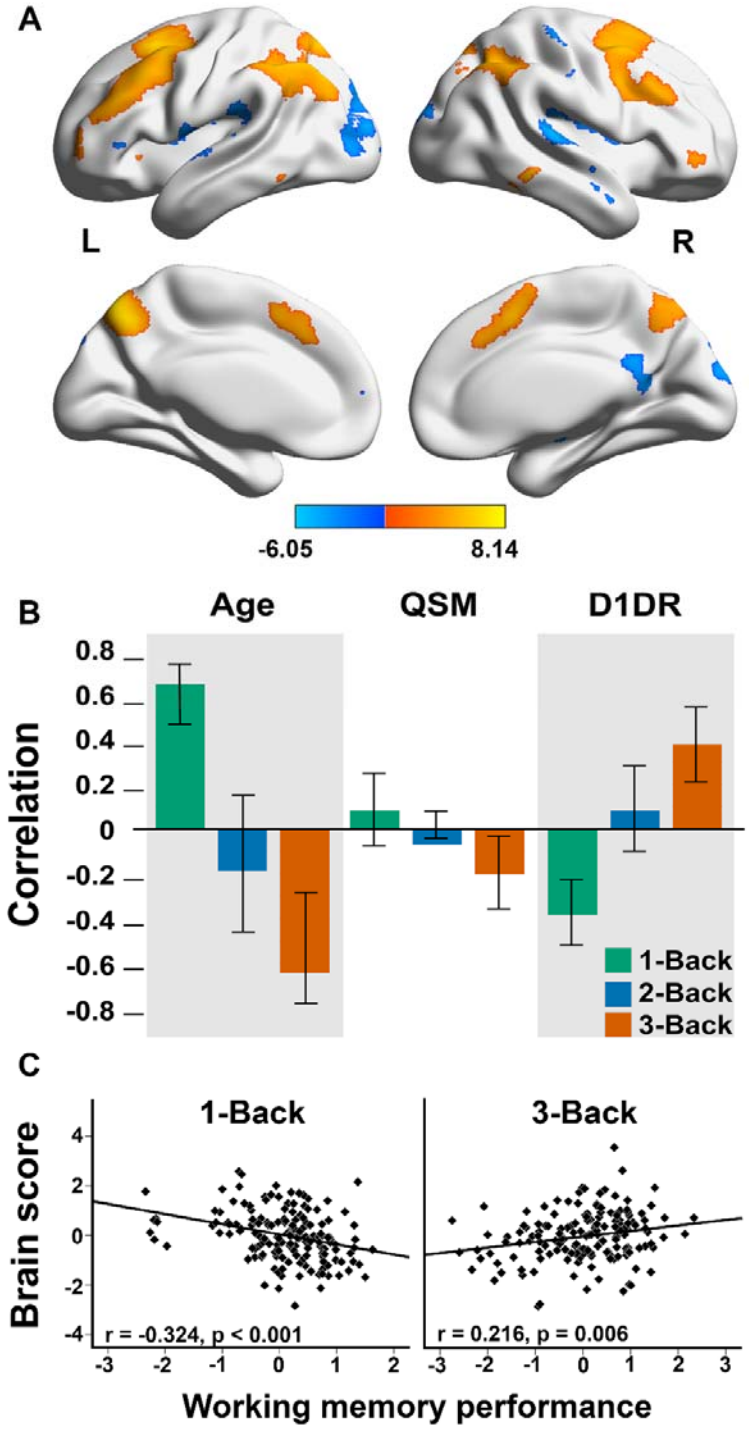

Figure 3. Multivariate relationship of BOLD response patterns during working-memory task identified by task PLS. **A)** The regions depicted in a yellow colour mainly correspond to the frontoparietal network, whereas the blue colour mainly represents the default-mode network. The frontoparietal network showed greater activation in correspondence to the behavioural measures across different task conditions, whereas the default-mode network showed greater deactivation (i.e., less activation). **B)** BOLD association across age, iron content (QSM), and D1DR. Interpretation of the figure should be as reliable positive and negative associations of activation (BOLD response) when the confidence intervals (CI:s) do not overlap with zero. As the frontoparietal network displayed increased activation, a positive association is interpreted as greater activation, whereas a negative

association is interpreted as less activation. For the default-mode network the opposite applies. **C)** Greater activation was associated with poorer performance during 1-back, but greater performance during 3-back. All values are z-transformed residuals adjusting for age.

3.4 Load-dependent BOLD response is differentially associated with task performance.

We have shown that increasing age was concomitant with increased and decreased activations within the frontoparietal network during 1-back and 3-back, respectively. We next tested the relationship of brain activation in relation to task performance. The brain score during 1-back was negatively associated with 1-back performance ($r = -0.324$, $p < 0.001$; Fig. 3C), but positively with 3-back ($r = 0.216$, $p = 0.006$; Fig. 3C). No significant association was observed during 2-back ($r = 0.05$, $p=0.4$). Taken together, our results suggest that less frontoparietal activity during 3-back as well as greater frontoparietal activity during 1-back are associated with less efficient working memory function.

3.5 Control analyses

To confirm that the results obtained from the partial correlation analyses were not due to confounding variables, we performed additional analyses in which we controlled for sex, education, and regional grey-matter volume. The inclusion of the additional variables did not result in a noticeable change of the outcome and all the patterns remained consistent. A full description of the results is given in the supplementary results.

4. Discussion

In this study, we provide first in-vivo evidence for an association between D1DR and brain iron across the adult lifespan, and how iron-D1DR synergy may contribute to disturbed brain responses during WM task performance across the lifespan. The main findings were that greater iron content was associated with lower D1DR in DLPFC, but not in striatum, across the adult lifespan. We also found that older individuals with elevated iron content and lower D1DR in DLPFC – a presumably deleterious synergy – exhibited lower frontoparietal activity along with less deactivation of the DMN

392 during high demand condition and in turn poorer WM performance. Although the associations
393 revealed by these data are cross-sectional, a plausible interpretation is that elevated iron and lower
394 D1DR together form a toxic couple (c.f. Hare & Double, 2016), which would contribute to reduced
395 network dynamics and impaired WM processing.

396 A key finding of the present study is the association between higher iron content and lower D1DR in
397 DLPFC across the adult lifespan. The exact mechanism underlying the association between iron
398 content and DA receptors is poorly understood. The dopaminergic system is important to cellular
399 iron homeostasis, as documented in *in vitro* studies (Dichtl et al., 2018; Liu et al., 2021). Supporting
400 this idea, we recently demonstrated that older adults with genetic predisposition for lower DA levels
401 accumulated more iron in DLPFC and striatum over time compared to individuals with presumably
402 higher DA levels (Gustavsson et al., 2022). Age-related differences in pre- and postsynaptic DA
403 markers (Bäckman et al., 2006, 2010) may also contribute to iron dyshomeostasis in aging, resulting
404 in disruption of transportation of iron via transferrin and storage in the ferritin protein (Ward et al.,
405 2014). Disruption of iron handling may lead to increase of ferrous iron, which triggers oxidative
406 stress, neuroinflammation, and cell loss due to ferroptosis (Daugherty et al., 2015; Mazhar et al.,
407 2021; Salami et al., 2021). The activation of D1 and D2/3 receptors alleviates oxidative stress-induced
408 inflammatory responses (Shao et al., 2013; Yan et al., 2015; Zhu et al., 2018). However, whether age-
409 related loss of DA receptors leads to an iron-related increase of oxidative stress and ferroptosis, or
410 whether an age-related increase of iron causes loss of DA receptor cells can only be determined in a
411 longitudinal setting.

412 We did not observe any significant association between iron and D1DR in striatum, except for a
413 trend-level negative association in older age. The reason for these regional variations is unclear. One
414 possibility is that, as D1DR are more expressed in striatum compared to cortex (Shohamy & Adcock,
415 2010), striatal regions are less vulnerable or better at attenuating the damage from higher iron
416 content. If too many receptors diminishes, or the threshold of the capacity for dealing with oxidative

417 stress is exceeded, the iron-induced damage to the cells may lead to ferroptosis (Lillig et al., 2008).
418 This concords well with Parkinson's Disease studies reporting regional variations in synuclein
419 pathology despite brain-wide iron accumulation (McCann et al., 2016), suggesting that additional
420 factors may contribute to iron serving a pathological role.

421 The multivariate PLS analysis revealed that in older age the combination of higher iron and lower
422 D1DR within DLPFC was related to high frontoparietal recruitment during low-demanding tasks along
423 with weak frontoparietal upregulation at higher task demand, which in turn was associated with
424 poorer working memory performance. These results concord with the Compensation-Related
425 Utilization of Neural Circuits Hypothesis (CRUNCH; (Cappell et al., 2010; Mattay et al., 2006; Nyberg
426 et al., 2014; Reuter-Lorenz & Cappell, 2008; Schneider-Garces et al., 2010)), which postulates that
427 neural activity increases at low demanding task-levels in older adults compared to younger adults,
428 but is reduced at more demanding levels.

429 The unique and shared contributions of iron content and neuroinflammation to astrocytic
430 dysfunction in the neurovascular coupling has been proposed to account for the reduced BOLD
431 response (Kalpouzos et al., 2017; Salami et al., 2018, 2021). Higher iron content has been related to
432 inflammation (Haider, 2015; Salami et al., 2021), which can be detrimental to cells during prolonged
433 periods (Hald & Lotharius, 2005; Zecca et al., 2004), thus contributing to astrocytic dysfunction. In
434 vitro studies have demonstrated that DA receptors activation may alleviate and supress
435 neuroinflammation (Liu et al., 2021; Shao et al., 2013; Yan et al., 2015). A more efficient
436 dopaminergic system (e.g., manifested by greater receptor availability) protect against negative
437 effects of iron and neuroinflammation on brain function. In support of this notion, a past study
438 showed that age-related D1DR alteration alone may contribute to less efficient engagement of
439 working memory circuits (Bäckman et al., 2011). Relatedly, the importance of DA for the
440 frontoparietal BOLD response has been further demonstrated through pharmacological
441 administration of a dopaminergic antagonist, leading to poorer working-memory performance

442 (Fischer et al., 2010). Our results add novel contribution to the previous work, by showing that the
443 combination of elevated iron and D1DR reduction in DLPFC in aging, possibly reflecting synergistic
444 iron-D1DR effects, exerts a deleterious effect in neural circuits of WM. Furthermore, during the most
445 demanding WM condition (3-back), lower activation in the frontoparietal network was related to
446 worse performance, in concordance with previous reports (Salami et al., 2021). Longitudinal data are
447 needed to identify the primary mechanism of disturbed working memory circuit in older age.

448 Our study is the first to link regional iron content to DA receptor availability, by showing that greater
449 iron content is related to lower D1DR. Critically, an interplay between age-related elevated iron
450 content and diminished D1 receptor availability may provide a mechanistic understanding of how
451 iron-DA coupling may exert deleterious effects on neural function and ultimately cognition. Elevated
452 brain iron has been implicated in several neurodegenerative disorders, including Parkinson's disease,
453 which is characterized by loss of dopaminergic cells (Ward et al., 2014). Thus, the observed findings
454 have implications for better understanding the mechanisms behind DA-related neurodegeneration.

455

456 **Author credit statement**

457 Conceptualisation: A.S. and G.K.; Software, M.A.; Methodology, J.G., G.K., G.P., A.S.; Formal Analysis
458 J.G., G.K., A.S., J.J., F.F., G.P., M.A., and B.A.P.; Visualisation, J.G. Writing – original draft, J.G., G.K.,
459 A.S., F.F.; Writing – Review & Editing G.P., J.J., L.A., B.A.P.

460 **Acknowledgement**

461 We thank the staff of the DyNAMiC project, Frida Magnusson and Emma Simonsson, staff at MRI and
462 PET labs at Umeå University Hospital, and all our participants. We also thank Robin Pedersen for his
463 contribution with the figures.

464 **Conflict of interest**

465 The authors declare no conflict of interest.

466 **Ethics approval**

467 This study was approved by the Regional Ethical board and the local Radiation Safety Committee in
468 Umeå, Sweden.

469 **Data availability statement**

470 Data from the DyNAMiC project cannot be made publicly available due to ethical and legal
471 restrictions. However, access to these original data may be available upon request from the
472 corresponding author.

473

474 **5. References**

475 Andrews-Hanna, J. R., Snyder, A. Z., Vincent, J. L., Lustig, C., Head, D., Raichle, M. E., & Buckner, R. L.
476 (2007). Disruption of Large-Scale Brain Systems in Advanced Aging. *Neuron*, *56*(5), 924–935.
477 https://doi.org/10.1016/j.neuron.2007.10.038

478 Ashburner, J. (2007). A fast diffeomorphic image registration algorithm. *NeuroImage*, *38*(1), 95–113.
479 https://doi.org/10.1016/j.neuroimage.2007.07.007

480 Bäckman, L., Ginovart, N., Dixon, R. A., Wahlin, T. B. R., Wahlin, Å., Halldin, C., & Farde, L. (2000).
481 Age-related cognitive deficits mediated by changes in the striatal dopamine system. *American*
482 *Journal of Psychiatry*, *157*(4), 635–637. https://doi.org/10.1176/appi.ajp.157.4.635

483 Bäckman, L., Karlsson, S., Fischer, H., Karlsson, P., Brehmer, Y., Rieckmann, A., MacDonald, S. W. S.,
484 Farde, L., & Nyberg, L. (2011). Dopamine D1 receptors and age differences in brain activation
485 during working memory. *Neurobiology of Aging*, *32*(10), 1849–1856.
486 https://doi.org/10.1016/j.neurobiolaging.2009.10.018

487 Bäckman, L., Nyberg, L., Lindenberger, U., Li, S. C., & Farde, L. (2006). The correlative triad among
488 aging, dopamine, and cognition: Current status and future prospects. *Neuroscience and*
489 *Biobehavioral Reviews*, *30*(6), 791–807. https://doi.org/10.1016/j.neubiorev.2006.06.005

490 Cappell, K. A., Gmeindl, L., & Reuter-Lorenz, P. A. (2010). Age differences in prefontal recruitment
491 during verbal working memory maintenance depend on memory load. *Cortex*, *46*(4), 462–473.
492 https://doi.org/10.1016/j.cortex.2009.11.009

493 Cass, W. A., Grondin, R., Andersen, A. H., Zhang, Z., Hardy, P. A., Hussey-Andersen, L. K., Rayens, W.
494 S., Gerhardt, G. A., & Gash, D. M. (2007). Iron accumulation in the striatum predicts aging-
495 related decline in motor function in rhesus monkeys. *Neurobiology of Aging*, *28*(2), 258–271.
496 https://doi.org/10.1016/j.neurobiolaging.2005.12.010

497 Cools, R., & D'Esposito, M. (2011). Inverted-U–Shaped Dopamine Actions on Human Working
498 Memory and Cognitive Control. *Biological Psychiatry*, *69*(12), e113–e125.
499 https://doi.org/https://doi.org/10.1016/j.biopsych.2011.03.028

500 Daugherty, A. M., Haacke, E. M., & Raz, N. (2015). Striatal iron content predicts its shrinkage and

changes in verbal working memory after two years in healthy adults. *Journal of Neuroscience*, *35*(17), 6731–6743. https://doi.org/10.1523/JNEUROSCI.4717-14.2015

Daugherty, A. M., & Raz, N. (2015). Appraising the Role of Iron in Brain Aging and Cognition: Promises and Limitations of MRI Methods. *Neuropsychology Review*, *25*(3), 272–287. https://doi.org/10.1007/s11065-015-9292-y

Daugherty, A. M., & Raz, N. (2016). Accumulation of iron in the putamen predicts its shrinkage in healthy older adults: A multi-occasion longitudinal study. *NeuroImage*, *128*(1), 11–20. https://doi.org/10.1016/j.neuroimage.2015.12.045

de Groot, M., Ikram, M. A., Akoudad, S., Krestin, G. P., Hofman, A., Lugt, A., Niessen, W. J., & Vernooij, M. W. (2015). Tract-specific white matter degeneration in aging: The Rotterdam Study. *Alzheimer's & Dementia*, *11*(3), 321–330. https://doi.org/10.1016/j.jalz.2014.06.011

Deistung, A., Schäfer, A., Schweser, F., Biedermann, U., Turner, R., & Reichenbach, J. R. (2013). Toward in vivo histology: A comparison of quantitative susceptibility mapping (QSM) with magnitude-, phase-, and R2*-imaging at ultra-high magnetic field strength. *NeuroImage*, *65*, 299–314. https://doi.org/10.1016/j.neuroimage.2012.09.055

Dichtl, S., Haschka, D., Nairz, M., Seifert, M., Volani, C., Lutz, O., & Weiss, G. (2018). Dopamine promotes cellular iron accumulation and oxidative stress responses in macrophages. *Biochemical Pharmacology*, *148*, 193–201. https://doi.org/10.1016/j.bcp.2017.12.001

Efron, B., & Tibshirani, R. (1986). Bootstrap Methods for Standard Errors, Confidence Intervals, and Other Measures of Statistical Accuracy. *Statistical Science*, *1*(1), 15–51. https://doi.org/10.1214/ss/1177013815

Erikson, K. M., Jones, B. C., Hess, E. J., Zhang, Q., & Beard, J. L. (2001). Iron deficiency decreases dopamine D1 and D2 receptors in rat brain. *Pharmacology Biochemistry and Behavior*, *69*(3–4), 409–418. https://doi.org/10.1016/S0091-3057(01)00563-9

Fischer, H., Nyberg, L., Karlsson, S., Karlsson, P., Brehmer, Y., Rieckmann, A., MacDonald, S. W. S., Farde, L., & Bäckman, L. (2010). Simulating Neurocognitive Aging: Effects of a Dopaminergic Antagonist on Brain Activity During Working Memory. *Biological Psychiatry*, *67*(6), 575–580. https://doi.org/10.1016/j.biopsych.2009.12.013

Fischl, B., Salat, D. H., Busa, E., Albert, M., Dieterich, M., Haselgrove, C., Van Der Kouwe, A., Killiany, R., Kennedy, D., Klaveness, S., Montillo, A., Makris, N., Rosen, B., & Dale, A. M. (2002). Whole brain segmentation: Automated labeling of neuroanatomical structures in the human brain. *Neuron*, *33*(3), 341–355. https://doi.org/10.1016/S0896-6273(02)00569-X

Fischl, B., Salat, D. H., Van Der Kouwe, A. J. W., Makris, N., Ségonne, F., Quinn, B. T., & Dale, A. M. (2004). Sequence-independent segmentation of magnetic resonance images. *NeuroImage*, *23*(SUPPL. 1), 69–84. https://doi.org/10.1016/j.neuroimage.2004.07.016

Fischl, B., Van Der Kouwe, A., Destrieux, C., Halgren, E., Ségonne, F., Salat, D. H., Busa, E., Seidman, L. J., Goldstein, J., Kennedy, D., Caviness, V., Makris, N., Rosen, B., & Dale, A. M. (2004). Automatically Parcellating the Human Cerebral Cortex. *Cerebral Cortex*, *14*(1), 11–22. https://doi.org/10.1093/cercor/bhg087

Garrett, D. D., Kovacevic, N., McIntosh, A. R., & Grady, C. L. (2010). Blood oxygen level-dependent signal variability is more than just noise. *Journal of Neuroscience*, *30*(14), 4914–4921. https://doi.org/10.1523/JNEUROSCI.5166-09.2010

Garzón, B., Sitnikov, R., Bäckman, L., & Kalpouzos, G. (2017). Can transverse relaxation rates in deep gray matter be approximated from functional and T2-weighted FLAIR scans for relative brain

iron quantification? *Magnetic Resonance Imaging*, *40*, 75–82. https://doi.org/10.1016/j.mri.2017.04.005

Gorbach, T., Pudas, S., Lundquist, A., Orädd, G., Josefsson, M., Salami, A., de Luna, X., & Nyberg, L. (2017). Longitudinal association between hippocampus atrophy and episodic-memory decline. *Neurobiology of Aging*, *51*, 167–176. https://doi.org/10.1016/j.neurobiolaging.2016.12.002

Grady, C. L., & Garrett, D. D. (2014). Understanding variability in the BOLD signal and why it matters for aging. *Brain Imaging and Behavior*, *8*(2), 274–283. https://doi.org/10.1007/s11682-013-9253-0

Gustavsson, J., Papenberg, G., Falahati, F., Laukka, E. J., & Kalpouzos, G. (2022). Contributions of the Catechol-O-Methyltransferase Val158Met Polymorphism to Changes in Brain Iron Across Adulthood and Their Relationships to Working Memory. *Frontiers in Human Neuroscience*, *16*. https://doi.org/10.3389/fnhum.2022.838228

Haider, L. (2015). Inflammation, Iron, Energy Failure, and Oxidative Stress in the Pathogenesis of Multiple Sclerosis. *Oxidative Medicine and Cellular Longevity*, *2015*(3), 1–10. https://doi.org/10.1155/2015/725370

Hald, A., & Lotharius, J. (2005). Oxidative stress and inflammation in Parkinson's disease: Is there a causal link? *Experimental Neurology*, *193*(2), 279–290. https://doi.org/10.1016/j.expneurol.2005.01.013

Hallgren, B., & Sourander, P. (1958). The Effect of Age on the Non-Haemin Iron in the Human Brain. *Journal of Neurochemistry*, *3*(1), 41–51. https://doi.org/10.1111/j.1471-4159.1958.tb12607.x

Hare, D. J., & Double, K. L. (2016). Iron and dopamine: A toxic couple. *Brain*, *139*(4), 1026–1035. https://doi.org/10.1093/brain/aww022

He, Y., Thong, P. S., Lee, T., Leong, S. ., Mao, B. Y., Dong, F., & Watt, F. (2003). Dopaminergic cell death precedes iron elevation in MPTP-injected monkeys. *Free Radical Biology and Medicine*, *35*(5), 540–547. https://doi.org/doi.org/10.1016/j.neurobiolaging.2005.12.010

Innis, R. B., Cunningham, V. J., Delforge, J., Fujita, M., Gjedde, A., Gunn, R. N., Holden, J., Houle, S., Huang, S.-C., Ichise, M., Iida, H., Ito, H., Kimura, Y., Koeppe, R. A., Knudsen, G. M., Knuuti, J., Lammertsma, A. A., Laruelle, M., Logan, J., … Carson, R. E. (2007). Consensus Nomenclature for in vivo Imaging of Reversibly Binding Radioligands. *Journal of Cerebral Blood Flow & Metabolism*, *27*(9), 1533–1539. https://doi.org/10.1038/sj.jcbfm.9600493

Johansson, J., Nordin, K., Pedersen, R., Karalija, N., Papenberg, G., Andersson, M., Korkki, S. M., Riklund, K., Guitart-Masip, M., Rieckmann, A., Bäckman, L., Nyberg, L., & Salami, A. (2022). Bi-phasic patterns of age-related differences in dopamine D1 receptors across the adult lifespan. *BioRxiv*, 1–35. https://doi.org/10.1101/2022.05.24.493225

Kalpouzos, G. (2018). Brain iron accumulation, and motor and cognitive decline in normal aging. *Revue de Neuropsychologie*, *10*(3), 205. https://doi.org/10.3917/rne.103.0205

Kalpouzos, G., Garzón, B., Sitnikov, R., Heiland, C., Salami, A., Persson, J., & Bäckman, L. (2017). Higher Striatal Iron Concentration is Linked to Frontostriatal Underactivation and Poorer Memory in Normal Aging. *Cerebral Cortex*, *27*(6), 3427–3436. https://doi.org/10.1093/cercor/bhx045

Karrer, T. M., Josef, A. K., Mata, R., Morris, E. D., & Samanez-Larkin, G. R. (2017). Reduced dopamine receptors and transporters but not synthesis capacity in normal aging adults: a meta-analysis. *Neurobiology of Aging*, *57*, 36–46. https://doi.org/10.1016/j.neurobiolaging.2017.05.006

588 Kaur, D., Yantiri, F., Rajagopalan, S., Kumar, J., Mo, J. Q., Boonplueang, R., Viswanath, V., Jacobs, R.,
589 Yang, L., Beal, M. F., DiMonte, D., Volitaskis, I., Ellerby, L., Cherny, R. A., Bush, A. I., & Andersen,
590 J. K. (2003). Genetic or Pharmacological Iron Chelation Prevents MPTP-Induced Neurotoxicity In
591 Vivo. *Neuron*, *37*(6), 899–909. https://doi.org/10.1016/S0896-6273(03)00126-0

592 Lammertsma, A. A., & Hume, S. P. (1996). Simplified Reference Tissue Model for PET Receptor
593 Studies. *NeuroImage*, *4*(3), 153–158. https://doi.org/10.1006/nimg.1996.0066

594 Landau, S. M., Lal, R., O'Neil, J. P., Baker, S., & Jagust, W. J. (2009). Striatal dopamine and working
595 memory. *Cerebral Cortex*, *19*(2), 445–454. https://doi.org/10.1093/cercor/bhn095

596 Langkammer, C., Schweser, F., Krebs, N., Deistung, A., Goessler, W., Scheurer, E., Sommer, K.,
597 Reishofer, G., Yen, K., Fazekas, F., Ropele, S., & Reichenbach, J. R. (2012). Quantitative
598 susceptibility mapping (QSM) as a means to measure brain iron? A post mortem validation
599 study. *NeuroImage*, *62*(3), 1593–1599. https://doi.org/10.1016/j.neuroimage.2012.05.049

600 Larsen, B., Olafsson, V., Calabro, F., Laymon, C., Tervo-Clemmens, B., Campbell, E., Minhas, D.,
601 Montez, D., Price, J., & Luna, B. (2020). Maturation of the human striatal dopamine system
602 revealed by PET and quantitative MRI. *Nature Communications*, *11*(1), 1–10.
603 https://doi.org/10.1038/s41467-020-14693-3

604 Leibovitch, F. S., Black, S. E., Caldwell, C. B., McIntosh, A. R., Ehrlich, L. E., & Szalai, J. P. (1999). Brain
605 SPECT imaging and left hemispatial neglect covaried using partial least squares: The sunnybrook
606 stroke study. *Human Brain Mapping*, *7*(4), 244–253. https://doi.org/10.1002/(SICI)1097-
607 0193(1999)7:4<244::AID-HBM3>3.0.CO;2-K

608 Li, W., Wu, B., Batrachenko, A., Bancroft-Wu, V., Morey, R. A., Shashi, V., Langkammer, C., De Bellis,
609 M. D., Ropele, S., Song, A. W., & Liu, C. (2014). Differential developmental trajectories of
610 magnetic susceptibility in human brain gray and white matter over the lifespan. *Human Brain*
611 *Mapping*, *35*(6), 2698–2713. https://doi.org/10.1002/hbm.22360

612 Lillig, C. H., Berndt, C., & Holmgren, A. (2008). Glutaredoxin systems. *Biochimica et Biophysica Acta -*
613 *General Subjects*, *1780*(11), 1304–1317. https://doi.org/10.1016/j.bbagen.2008.06.003

614 Liu, T., Liu, J., De Rochefort, L., Spincemaille, P., Khalidov, I., Ledoux, J. R., & Wang, Y. (2011).
615 Morphology enabled dipole inversion (MEDI) from a single-angle acquisition: Comparison with
616 COSMOS in human brain imaging. *Magnetic Resonance in Medicine*, *66*(3), 777–783.
617 https://doi.org/10.1002/mrm.22816

618 Liu, T., Wisnieff, C., Lou, M., Chen, W., Spincemaille, P., & Wang, Y. (2013). Nonlinear formulation of
619 the magnetic field to source relationship for robust quantitative susceptibility mapping.
620 *Magnetic Resonance in Medicine*, *69*(2), 467–476. https://doi.org/10.1002/mrm.24272

621 Liu, Z., Zhai, X. R., Du, Z. S., Xu, F. F., Huang, Y., Wang, X. Q., Qiu, Y. H., & Peng, Y. P. (2021). Dopamine
622 receptor D2 on CD4+ T cells is protective against neuroinflammation and neurodegeneration in
623 a mouse model of Parkinson's disease. *Brain, Behavior, and Immunity*, *98*(April), 110–121.
624 https://doi.org/10.1016/j.bbi.2021.08.220

625 Mattay, V. S., Fera, F., Tessitore, A., Hariri, A. R., Berman, K. F., Das, S., Meyer-Lindenberg, A.,
626 Goldberg, T. E., Callicott, J. H., & Weinberger, D. R. (2006). Neurophysiological correlates of age-
627 related changes in working memory capacity. *Neuroscience Letters*, *392*(1–2), 32–37.
628 https://doi.org/10.1016/j.neulet.2005.09.025

629 Mazhar, M., Din, A. U., Ali, H., Yang, G., Ren, W., Wang, L., Fan, X., & Yang, S. (2021). Implication of
630 ferroptosis in aging. *Cell Death Discovery*, *7*(1), 1–9. https://doi.org/10.1038/s41420-021-
631 00553-6

McCann, H., Cartwright, H., & Halliday, G. M. (2016). Neuropathology of α-synuclein propagation and braak hypothesis. *Movement Disorders*, *31*(2), 152–160. https://doi.org/10.1002/mds.26421

McIntosh, A. R., Bookstein, F. L., Haxby, J. V., & Grady, C. L. (1996). Spatial pattern analysis of functional brain images using partial least squares. *NeuroImage*, *3*(3 I), 143–157. https://doi.org/10.1006/nimg.1996.0016

McIntosh, A. R., Chau, W. K., & Protzner, A. B. (2004). Spatiotemporal analysis of event-related fMRI data using partial least squares. *NeuroImage*, *23*(2), 764–775. https://doi.org/10.1016/j.neuroimage.2004.05.018

McIntosh, A. R., & Lobaugh, N. J. (2004). Partial least squares analysis of neuroimaging data: Applications and advances. *NeuroImage*, *23*(SUPPL. 1), 250–263. https://doi.org/10.1016/j.neuroimage.2004.07.020

Mills, E., Dong, X. P., Wang, F., & Xu, H. (2010). Mechanisms of brain iron transport: Insight into neurodegeneration and CNS disorders. *Future Medicinal Chemistry*, *2*(1), 51–64. https://doi.org/10.4155/fmc.09.140

Nordin, K., Gorbach, T., Pedersen, R., Lundmark, V. P., Johansson, J., Andersson, M., Mcnulty, C., Riklund, K., Wåhlin, A., Papenberg, G., Kalpouzos, G., Bäckman, L., & Salami, A. (2022). DyNAMiC: A prospective longitudinal study of dopamine and brain connectomes: A new window into cognitive aging. *Journal of Neuroscience Research*, *January*, 1–25. https://doi.org/10.1002/jnr.25039

Nyberg, L., Andersson, M., Forsgren, L., Jakobsson-Mo, S., Larsson, A., Marklund, P., Nilsson, L. G., Riklund, K., & Bäckman, L. (2009). Striatal dopamine D2 binding is related to frontal BOLD response during updating of long-term memory representations. *NeuroImage*, *46*(4), 1194–1199. https://doi.org/10.1016/j.neuroimage.2009.03.035

Nyberg, L., Andersson, M., Kauppi, K., Lundquist, A., Persson, J., Pudas, S., & Nilsson, L.-G. (2014). Age-related and Genetic Modulation of Frontal Cortex Efficiency. *Journal of Cognitive Neuroscience*, *26*(4), 746–754. https://doi.org/10.1162/jocn_a_00521

Nyberg, L., Dahlin, E., Stigsdotter Neely, A., & BÄckman, L. (2009). Neural correlates of variable working memory load across adult age and skill: Dissociative patterns within the fronto-parietal network: Cognition and Neurosciences. *Scandinavian Journal of Psychology*, *50*(1), 41–46. https://doi.org/10.1111/j.1467-9450.2008.00678.x

Ortega, R., Cloetens, P., Devès, G., Carmona, A., & Bohic, S. (2007). Iron storage within dopamine neurovesicles revealed by chemical nano-imaging. *PLoS ONE*, *2*(9). https://doi.org/10.1371/journal.pone.0000925

Poetini, M. R., Araujo, S. M., Trindade de Paula, M., Bortolotto, V. C., Meichtry, L. B., Polet de Almeida, F., Jesse, C. R., Kunz, S. N., & Prigol, M. (2018). Hesperidin attenuates iron-induced oxidative damage and dopamine depletion in Drosophila melanogaster model of Parkinson's disease. *Chemico-Biological Interactions*, *279*(September 2017), 177–186. https://doi.org/10.1016/j.cbi.2017.11.018

Reuter-Lorenz, P. A., & Cappell, K. A. (2008). Neurocognitive aging and the compensation hypothesis. *Current Directions in Psychological Science*, *17*(3), 177–182. https://doi.org/10.1111/j.1467-8721.2008.00570.x

Rieckmann, A., Karlsson, S., Karlsson, P., Brehmer, Y., Fischer, H., Farde, L., Nyberg, L., & Bäckman, L. (2011). Dopamine D1 receptor associations within and between dopaminergic pathways in younger and elderly adults: Links to cognitive performance. *Cerebral Cortex*, *21*(9), 2023–2032.

https://doi.org/10.1093/cercor/bhq266

Rodrigue, K. M., Daugherty, A. M., Foster, C. M., & Kennedy, K. M. (2020). Striatal iron content is linked to reduced fronto-striatal brain function under working memory load. *NeuroImage*, *210*(October 2019), 116544. https://doi.org/10.1016/j.neuroimage.2020.116544

Salami, A., Avelar-Pereira, B., Garzón, B., Sitnikov, R., & Kalpouzos, G. (2018). Functional coherence of striatal resting-state networks is modulated by striatal iron content. *NeuroImage*, *183*(April), 495–503. https://doi.org/10.1016/j.neuroimage.2018.08.036

Salami, A., Eriksson, J., Kompus, K., Habib, R., Kauppi, K., & Nyberg, L. (2010). Characterizing the neural correlates of modality-specific and modality-independent accessibility and availability signals in memory using partial-least squares. *NeuroImage*, *52*(2), 686–698. https://doi.org/10.1016/j.neuroimage.2010.04.195

Salami, A., Eriksson, J., & Nyberg, L. (2012). Opposing effects of aging on large-scale Brain systems for memory encoding and cognitive control. *Journal of Neuroscience*, *32*(31), 10749–10757. https://doi.org/10.1523/JNEUROSCI.0278-12.2012

Salami, A., Garrett, D. D., Wåhlin, A., Rieckmann, A., Papenberg, G., Karalija, N., Jonasson, L., Andersson, M., Axelsson, J., Johansson, J., Riklund, K., Lövdén, M., Lindenberger, U., Bäckman, L., & Nyberg, L. (2019). Dopamine D 2/3 binding potential modulates neural signatures of working memory in a load-dependent fashion. *Journal of Neuroscience*, *39*(3), 537–547. https://doi.org/10.1523/JNEUROSCI.1493-18.2018

Salami, A., Papenberg, G., Sitnikov, R., Laukka, E. J., Persson, J., & Kalpouzos, G. (2021). Elevated Neuroinflammation Contributes to the Deleterious Impact of Iron Overload on Brain Function in Aging. *NeuroImage*, *230*(August 2020), 117792. https://doi.org/10.1016/j.neuroimage.2021.117792

Salami, A., Rieckmann, A., Fischer, H., & Bäckman, L. (2014). A multivariate analysis of age-related differences in functional networks supporting conflict resolution. *NeuroImage*, *86*, 150–163. https://doi.org/10.1016/j.neuroimage.2013.08.002

Salthouse, T. (2012). Consequences of age-related cognitive declines. Annual review of psychology. *Annu Rev Psychol.*, *63*, 201-226. https://doi.org/10.1146/annurev-psych-120710-100328.Consequences

Schneider-Garces, N. J., Gordon, B. A., Brumback-Peltz, C. R., Shin, E., Lee, Y., Sutton, B. P., Maclin, E. L., Gratton, G., & Fabiani, M. (2010). Span, CRUNCH, and beyond: Working memory capacity and the aging brain. *Journal of Cognitive Neuroscience*, *22*(4), 655–669. https://doi.org/10.1162/jocn.2009.21230

Shao, W., Zhang, S., Tang, M., Zhang, X., Zhou, Z., Yin, Y., Zhou, Q., Huang, Y., Liu, Y., Wawrousek, E., Chen, T., Li, S., Xu, M., Zhou, J., Hu, G., & Zhou, J. (2013). Suppression of neuroinflammation by astrocytic dopamine D2 receptors via αB-crystallin. *Nature*, *494*, 90–94. https://doi.org/https://doi.org/10.1038/nature11748

Shohamy, D., & Adcock, R. A. (2010). Dopamine and adaptive memory. *Trends in Cognitive Sciences*, *14*(10), 464–472. https://doi.org/10.1016/j.tics.2010.08.002

Spence, H., McNeil, C. J., & Waiter, G. D. (2020). The impact of brain iron accumulation on cognition: A systematic review. *PLoS ONE*, *15*(10 October). https://doi.org/10.1371/journal.pone.0240697

Steiger, T. K., Weiskopf, N., & Bunzeck, N. (2016). Iron level and myelin content in the ventral striatum predict memory performance in the aging brain. *Journal of Neuroscience*, *36*(12), 3552–3558. https://doi.org/10.1523/JNEUROSCI.3617-15.2016

Straub, S., Schneider, T. M., Emmerich, J., Freitag, M. T., Ziener, C. H., Schlemmer, H. P., Ladd, M. E., & Laun, F. B. (2017). Suitable reference tissues for quantitative susceptibility mapping of the brain. *Magnetic Resonance in Medicine*, *78*(1), 204–214. https://doi.org/10.1002/mrm.26369

Tabachnick, B., & Fidell, L. (2013). Using Multivariate Statistics. In *Singular Spectrum Analysis* (6th ed.). Pearson. https://doi.org/10.1007/978-1-4757-2514-8_3

Unger, E. L., Bianco, L. E., Jones, B. C., Allen, R. P., & Earley, C. J. (2014). Low brain iron effects and reversibility on striatal dopamine dynamics. *Experimental Neurology*, *261*, 462–468. https://doi.org/10.1016/j.expneurol.2014.06.023

Ward, R. J., Zucca, F. A., Duyn, J. H., Crichton, R. R., & Zecca, L. (2014). The role of iron in brain ageing and neurodegenerative disorders. *The Lancet Neurology*, *13*(10), 1045–1060. https://doi.org/10.1016/S1474-4422(14)70117-6

Xu, W., & Cumming, I. (1999). A region-growing algorithm for InSAR phase unwrapping. *IEEE Transactions on Geoscience and Remote Sensing*, *37*(1), 124–134. https://doi.org/10.1109/36.739143

Yan, Y., Jiang, W., Liu, L., Wang, X., Ding, C., Tian, Z., & Zhou, R. (2015). Dopamine Controls Systemic Inflammation through Inhibition of NLRP3 Inflammasome. *Cell*, *160*(1–2), 62–73. https://doi.org/10.1016/j.cell.2014.11.047

Youdim, M. B. H., Ben-Shachar, D., & Riederer, P. (1993). The possible role of iron in the etiopathology of parkinson's disease. *Movement Disorders*, *8*(1), 1–12. https://doi.org/10.1002/mds.870080102

Zecca, L., Youdim, M., Riederer, P., Connor, J. R., & Crichton, R. R. (2004). Iron, brain ageing and neurodegenerative disorders. *Nature Reviews Neuroscience*, *5*(11), 863–873. https://doi.org/10.1038/nrn1537

Zhu, J., Hu, Z., Han, X., Wang, D., Jiang, Q., Ding, J., Xiao, M., Wang, C., Lu, M., & Hu, G. (2018). Dopamine D2 receptor restricts astrocytic NLRP3 in fl ammasome activation via enhancing the interaction of β -arrestin2 and NLRP3. *Cell Death & Differentiation*, *25*, 2037–2049. https://doi.org/10.1038/s41418-018-0127-2

Zimmerman, M. E., Brickman, A. M., Paul, R. H., Grieve, S. M., Tate, D. F., Gunstad, J., Cohen, R. A., Aloia, M. S., Williams, L. M., Clark, C. R., Whitford, T. J., & Gordon, E. (2006). The relationship between frontal gray matter volume and cognition varies across the healthy adult lifespan. *American Journal of Geriatric Psychiatry*, *14*(10), 823–833. https://doi.org/10.1097/01.JGP.0000238502.40963.ac

Zucca, F. A., Segura-Aguilar, J., Ferrari, E., Muñoz, P., Paris, I., Sulzer, D., Sarna, T., Casella, L., & Zecca, L. (2017). Interactions of iron, dopamine and neuromelanin pathways in brain aging and Parkinson's disease. *Progress in Neurobiology*, *155*(3), 96–119. https://doi.org/10.1016/j.pneurobio.2015.09.012